Tailoring nanopore formation in atomic layer deposited ultrathin films

Tailoring nanopore formation in atomic layer deposited ultrathin films

Saurabh Karwal, Tao Li, Angel Yanguas-Gil, Christian P. Canlas, Yu Lei, Anil U. Mane, Joseph A. Libera, Soenke Seifert, Randall E. Winans, and Jeffrey W. Elam

Citation: Journal of Vacuum Science & Technology A: Vacuum, Surfaces, and Films **36**, 01A103 (2018);

View online: https://doi.org/10.1116/1.5003360

View Table of Contents: http://avs.scitation.org/toc/jva/36/1

Published by the American Vacuum Society

Tailoring nanopore formation in atomic layer deposited ultrathin films

Saurabh Karwal
Department of Applied Physics, University of Technology Eindhoven, P.O. Box 503, Eindhoven 5600MB

Tao Li,
X-ray Science Division, Argonne National Laboratory, Argonne, Illinois 60439

Angel Yanguas-Gil and Christian P. Canlas
Energy Systems Division, Argonne National Laboratory, Argonne, Illinois 60439

Yu Lei
Department of Chemical and Materials Engineering, University of Alabama in Huntsville, Huntsville, Alabama 35899

Anil U. Mane and Joseph A. Libera
Energy Systems Division, Argonne National Laboratory, Argonne, Illinois 60439

Soenke Seifert and Randall E. Winans
X-ray Science Division, Argonne National Laboratory, Argonne, Illinois 60439

Jeffrey W. Elam[a)]
Energy Systems Division, Argonne National Laboratory, Argonne, Illinois 60439

(Received 5 September 2017; accepted 16 October 2017; published 15 November 2017)

Selectivity is a critical attribute of catalysts used in manufacturing of essential and fine chemicals. An excellent way to induce selectivity in catalysts is by using ultrathin films with tailored nanoporosity. For instance, nanopores can be created in atomic layer deposition (ALD) ultrathin over-coatings on supported metal nanoparticles by subjecting the coatings to high temperature annealing. These nanopores expose the active surface of the underlying metal nanoparticles. The dimensions of these nanopores can be tuned to impart shape selectivity: only reactants or products with a specific size or shape can fit inside the pore. In this work, the authors explore the underlying mechanism driving nanopore formation in ALD films. Ultrathin films of ALD TiO_2 (~2.5 nm thick) and ALD Al_2O_3 (~4.9 nm thick) were deposited on nonporous γ-Al_2O_3 nanoparticles. The pore formation and evolution were monitored *in situ* during thermal annealing using small-angle x-ray scattering (SAXS), and the crystallinity was monitored by *in situ* x-ray diffraction. A correlation between the nanopore formation and amorphous to crystalline phase transitions in the ALD layers was observed. The authors hypothesize that the pores form through the relaxation of stress induced by densification of the ALD films during the phase transitions. The authors developed a mathematical model to evaluate this hypothesis and found remarkable agreement between the model and the SAXS measurements. https://doi.org/10.1116/1.5003360

I. INTRODUCTION

The deactivation of supported noble metal nanoparticle (NP) catalysts due to coking, leaching, and sintering is a major issue that necessitates expensive and periodic catalyst regeneration. These supported NP catalysts can be stabilized against sintering at elevated temperatures by over-coating them with ultrathin metal oxide layers using atomic layer deposition (ALD).[1–3] Besides stabilization, Feng *et al*. and O'Neill *et al*. demonstrated that the over-coated catalysts can retain their activity when coated with ultrathin Al_2O_3 ALD layers (2–4 nm).[3,4] Furthermore, Lu *et al*. demonstrated that shape-selectivity can be induced in NP catalysts over-coated with Al_2O_3 ALD layers by high temperature, postdeposition annealing.[2] In the same work, a relatively thick Al_2O_3 ALD layer was applied that completely covered the underlying catalyst NPs. Upon calcination at elevated temperatures, nanopores formed in the ALD film, which exposed the underlying catalyst surface as well as inducing shape-selectivity.[2] However, the mechanism of pore formation in the ALD over-coat layers has not been investigated. Understanding the mechanism of pore formation may facilitate the development of new shape-selective catalysts.

In situ synchrotron techniques such as small-angle- and wide-angle x-ray scattering (SAXS and WAXS) are extremely useful for studying the formation of nanopores in supported NP catalyst systems over-coated with ALD layers.[5,6] Recently, we showed that SAXS/WAXS can provide useful insights for understanding the underlying mechanism of nanopore formation in ultrathin ALD layers.[7] In this previous study, ALD Al_2O_3 and TiO_2 were deposited on nonporous, spherical γ-Al_2O_3 nanoparticles and studied using SAXS/WAXS after *ex situ* annealing at temperatures up to ~800 °C to investigate nanopore formation. This study found that nanopore formation in the ALD layers is correlated with amorphous to crystalline phase transitions.[7]

In this work, we present an in-depth study of the mechanism of nanopore formation combining *in situ* SAXS and

[a)]Electronic mail: jelam@anl.gov

x-ray diffraction (XRD) during high temperature annealing with mathematical modeling. The formation of nanopores, pore size distribution, and the phase transition in the ALD TiO_2 and ALD Al_2O_3 layers as a function of annealing temperature were studied in detail. We discovered that the nanopore formation temperature coincided with the amorphous to crystalline phase transition temperature for both the ALD layers. Furthermore, we found that the nanopore size increases with annealing temperature and is an irreversible phenomenon. We hypothesize that the densification in thin ALD layers stemming from crystallization and thermal mismatch between the film and the substrate induces lateral stress in the film, which, upon relaxation, leads to the formation of nanopores. A mathematical model was developed to further support this hypothesis of nanopore formation,[8,9] and the results from the model agreed remarkably well with the *in situ* SAXS measurements.

II. EXPERIMENT

A. Film deposition

The ALD of TiO_2 (~2.5 nm thick) and Al_2O_3 (~4.9 nm thick) ultrathin films was conducted in a hot-walled, viscous flow reactor constructed with a circular stainless steel tube having an internal diameter of 5 cm as described in detail in Ref. 10. Ultrahigh purity (99.999%) nitrogen carrier gas was constantly passed through the reactor at a flow rate of 400 sccm, resulting in a steady-state pressure of 1 Torr inside the reactor chamber.

Commercially available nonporous spherical γ-Al_2O_3 nanoparticles with a specific surface area of 40 m^2/g (NanoDur, 99.5%, Alfa Aesar) were used in this study. The NanoDur powder was examined by transmission electron microscopy (TEM) using a JEOL 3010 TEM microscope. Figure 1(a) shows a TEM image of the as-received NanoDur substrate. Phase transitions in the NanoDur substrate could complicate the interpretation of the SAXS measurements used to monitor the nanopore formation in the ALD layers. Consequently, the nanoparticles were calcined at 1000 °C for 3 h in a Thermolyne type 48000 furnace in air prior to the ALD to crystallize the substrate fully so that it remained stable during the *in situ* annealing experiments. The inset in the TEM image of the calcined NanoDur [Fig. 1(b)] reveals sharp facets (black arrows) that form during crystallization. TEM revealed a broad particle size distribution for the calcined NanoDur substrate with an approximate mean particle diameter of 40 nm [Fig. 1(c)], which is used in the model calculations. Approximately 1.5 g of calcined NanoDur was placed in a shallow tray covered with a tight-fitting wire cloth lid to contain the powder without restricting diffusion of ALD precursors.[11] After loading the powder, the calcined NanoDur was allowed to thermally equilibrate and outgas at 200 °C for 10 min, after which the surface was cleaned using a 15 min exposure to ozone produced by using a commercial ozone generator (Ozone Engineering L11) using a feed of ultrahigh purity oxygen at a flow rate of 400 sccm and a pressure of 1 Torr to produce ~10% ozone in oxygen.

The TiO_2 ALD was performed using alternating exposures to titanium isopropoxide (TTIP, Aldrich) and deionized water (H_2O, 18 MΩ cm) at a reactor temperature of 200 °C. The TTIP was contained in a stainless steel bubbler heated to 80 °C and transported to the substrate using a N_2 gas flow of 40 sccm. H_2O was held in a glass reservoir at room temperature and was injected into a N_2 flow of 20 sccm. Under saturation conditions, the TTIP and H_2O dosing time of 90 s and purge time of 120 s were used. A total of 85 TiO_2 ALD cycles were performed, yielding a film thickness of ~2.5 nm based on the growth per cycle (GPC) literature value of 0.3 Å/cycle.[12] The Al_2O_3 ALD was performed using alternating exposures to trimethylaluminum (TMA, Aldrich, 95%) and H_2O at a reactor temperature of 200 °C. The TMA was contained in a stainless steel reservoir at room temperature. Both TMA and H_2O were injected into a N_2 flow of 50 sccm. The precursor and coreactant saturation was achieved using the TMA and H_2O dose time of 50 s and purge time of 70 s. Forty five Al_2O_3 ALD cycles were performed giving a film thickness of ~4.9 nm using a GPC literature value of 1.1 Å/cycle.[13] The purge times for Al_2O_3 ALD are smaller than

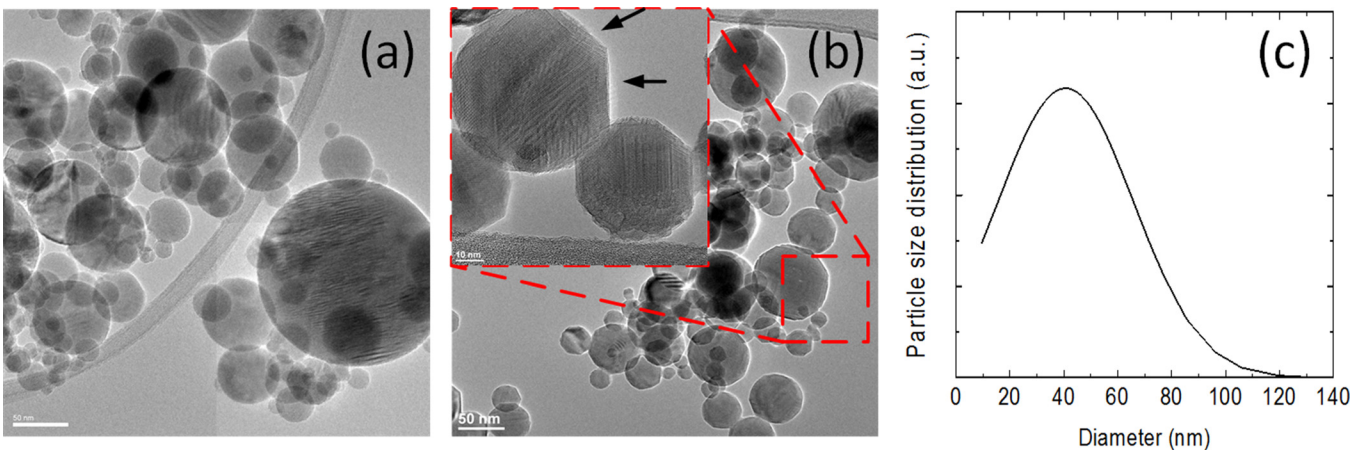

FIG. 1. (Color online) TEM images of γ-Al_2O_3 nanoparticles (a) as-received revealing nonporous, smooth spherical nanoparticles, (b) after annealing at 1000 °C for 3 h in air where sharp facets can be seen (black arrows), and (c) particle size distribution of the calcined nanoparticles computed from the TEM images.

those for TiO_2 ALD due to the much lower vapor pressure of the isopropyl alcohol reaction product for TiO_2 ALD compared to the methane reaction product for Al_2O_3 ALD.

B. Film characterization

Nanopore formation in the ALD thin films was studied using SAXS at beamlines 12-ID-B and 12-ID-C at the *Advanced Photon Source* (APS) of the Argonne National Laboratory using an x-ray energy of 14 keV. The two-dimensional (2D) images were radially averaged to produce 1D plots of scattered intensity $I(q)$ versus q, where $q = 4\pi(\sin\theta)/\lambda$. A Pilatus 2M detector (Dectris Ltd.) was used to acquire scattering data with typical exposure times in the range of 0.1–1.0 s. Samples were pressed into wafers, and the formed pellet was held inside a Linkam stage (TS1500) for *in situ* measurements. The samples were heated to 1000 °C using a heating rate of 20 °C/min, held for 10 min at 1000 °C, and then cooled to room temperature at a rate of 20 °C/min. The SAXS data were analyzed and fitted using Irena software.[14]

Phase transitions in the ALD over-coatings were studied using *in situ* synchrotron XRD at the 11-ID-C beamline at the APS. Samples were pressed into wafers, and the formed pellet was held inside a Linkam stage (TS1500) for *in situ* measurements. 2D XRD patterns were collected in the transmission mode with radiation with a high energy of 115 keV with typical exposure times in the range of 5–10 s. The collected 2D patterns were integrated to obtain conventional 1D patterns (intensity versus 2θ) and analyzed using the FIT2D software.

Thermogravimetric analysis was performed using an STA 449 F3 Jupiter (Netzsch). Approximately 20 mg of sample was placed in a closed alumina crucible (85 μl). The temperature was ramped up from 35 to 850 °C at a heating rate of 10 °C/min, and the mass loss was recorded under a dynamic flow of air (50 ml/min).

C. Mathematical model

A mathematical model (see supplementary material for details)[24] was developed to predict the size of the nanopores formed in the ALD over-coatings during annealing. We hypothesize that stresses are induced in the thin films because of film densification due to phase transition and/or thermal mismatch, which, upon relaxation, leads to nanopore formation (Fig. 2).

Figure 2(a) depicts the unstrained condition where the ALD film rests on the NanoDur substrate. Upon annealing, the ALD film densifies and contracts, whereas the substrate thermally expands [Fig. 2(b)]. As a consequence, the film deforms laterally to maintain the dimension of the substrate, and this produces tangential stress[15] which is relieved by pore formation. The final film volume and density can be computed using the conservation of mass (see supplementary material, Fig. S2). The nanopore radius (r_p) can be expressed as

$$r_p^2 = \frac{b^2\{1 + 2 \times \alpha_{s,l} \times \Delta T\}h' - b^2 a \times \frac{\rho_{f,25C}}{\rho_{f,TC}}}{n\pi h'}, \tag{1}$$

where b is the initial substrate length, a is the initial ALD film thickness, $\alpha_{s,l}$ is the thermal expansion coefficient of the substrate, ΔT is the temperature increase, h' is the final film height after deformation, $\rho_{f,25\,C}$ and $\rho_{f,TC}$ are the initial and final ALD film density, and n is the number of pores.

The total nanopore volume is subtracted from the deformed film [Fig. S2(b)] to obtain the final film volume as depicted in Fig. S2(c). Consequently, the developed stress is allowed to relax in n number of identical cylindrical pores and is expressed by

$$n = \frac{\frac{E_f}{(1-\nu_f)}\left[\frac{(1-\nu_f)+\sqrt{(1-\nu_f)(1+7\nu_f)}}{4\nu_f} - 1 + (\alpha_{s,l} - \alpha_{f,l})\Delta T\right]}{\frac{E_s}{(1-\nu_s)(1-2\nu_s)}\left[\{1 + 2 \times \alpha_{s,l} \times \Delta T\}^{1/2} - 1\right]} - 1, \tag{2}$$

where E_f and E_s are the Young's moduli of the film and the substrate, respectively, ν_f and ν_s are Poisson's ratio of the film and the substrate, respectively, and $\alpha_{f,l}$ is the thermal expansion coefficient of the film. Furthermore, nanopore formation in thin films should be dictated by minimization of the Gibbs surface free energy, leading to

$$h' + r_p\frac{dh'}{dr_p} - 2r_p = 0. \tag{3}$$

Equations (1)–(3) are solved to obtain the nanopore radius, r_p. We assume a phase transition in the ultrathin ALD layers from amorphous to crystalline. The ALD film densities and mechanical constants are taken from the literature (see supplementary material).[8,12,13,16–21] Although our model assumes a step change in the ALD film density at the phase transition temperature, these density changes can be gradual and smooth depending on the degree of crystallinity and necessitate a more complex model.

III. RESULTS AND DISCUSSION

A. TiO_2 and Al_2O_3 ALD

Our first experiments established the dose and purge times necessary for self-limiting TiO_2 and Al_2O_3 ALD on the nanoparticle substrates. Figure 3(a) shows the

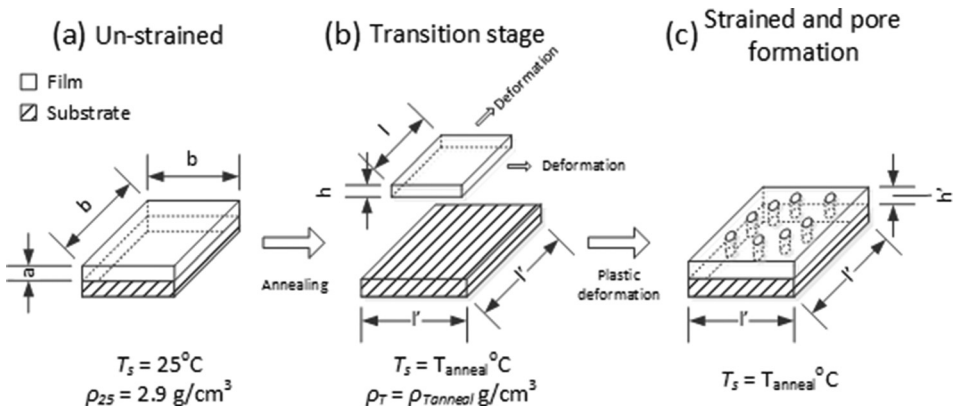

FIG. 2. Mechanism of nanopore formation in the thin ALD film. (a) Initially, the film has the same dimensions as the substrate, (b) film densification occurs that stems from phase transition, and (c) nanopore formation takes place because of compressive stress relaxation.

experimental percentage weight gain for 1.5 g of calcined γ-Al_2O_3 nanoparticles after 5 ALD TiO_2 cycles as a function of the TTIP dosing time from 0 to 150 s. For these experiments, the H_2O dose time was set to 150 s and a purge time of 200 s was used, giving the timing sequence: x–200–150–200. Figure 3(a) shows that the percentage weight gain saturates at ~2.7% after 80 s of TTIP dose.

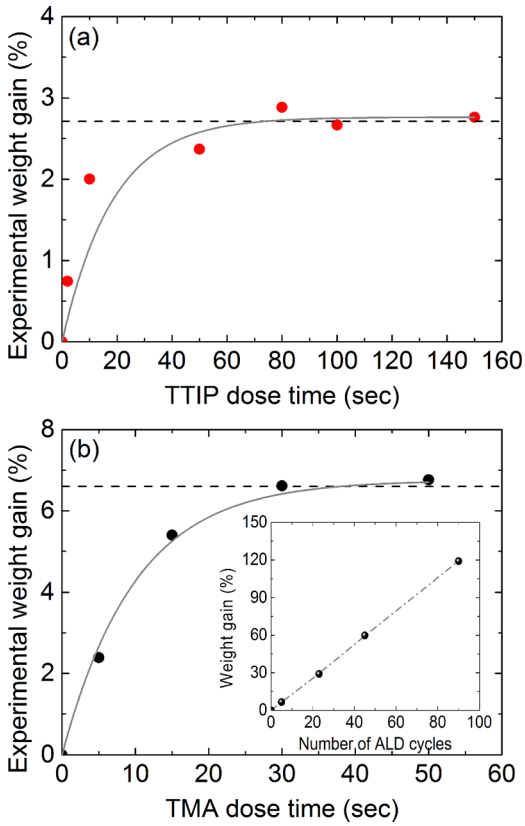

FIG. 3. (Color online) Precursor saturation measurements performed on 1.5 g of calcined γ-Al_2O_3 nanoparticles investigated by weight gain measurements for (a) TiO_2 ALD using 5 cycles TTIP/H_2O and (b) Al_2O_3 ALD using 5 cycles TMA/H_2O with the inset depicting linear weight gain % as a function of number of Al_2O_3 ALD cycles. The horizontal black dashed lines represent the expected saturation weight gain values, and the solid gray lines are fits with a Langmuir adsorption function.

Furthermore, the weight gain data were fit well using a Langmuir adsorption model with a time constant of 18.5 s [solid line in Fig. 3(a)]. The expected weight gain can be calculated using the literature values for TiO_2 ALD of GPC = 0.4 Å/cycle and density = 3.39 g/cm^3 and the calcined NanoDur BET surface area of 40 m^2/g (see supplementary material for details).[18] These values yield a theoretical weight gain of 2.71% [horizontal dashed line in Fig. 3(a)] in excellent agreement with the experimental value. In a similar fashion, we determined that a H_2O dose time of 80 s and a purge time of 120 s were sufficient for self-limiting TiO_2 ALD (not shown). Consequently, the timing sequence 90–120–90–120 was used for all the TiO_2 ALD on NanoDur.

Figure 3(b) shows the percentage weight gain for 1.5 g of NanoDur after 5 ALD Al_2O_3 cycles versus the TMA dose time between 0 and 50 s using the timing sequence x–120–100–120. The Al_2O_3 ALD saturates at a weight gain of ~6.7% after a 30 s TMA dose and is well fit with a Langmuir adsorption function using a time constant of 10 s. We attribute the smaller time constant for TMA adsorption as compared to TTIP mainly to the higher vapor pressure of the TMA. The expected weight gain calculated from the Al_2O_3 ALD literature values of GPC = 1.1 Å/cycle and density = 3.0 g/cm^3 is 6.6% (see supplementary material for details), in very close agreement with the experiment.[17] Additional measurements (not shown) established that 30 s H_2O exposures and 70 s purge times yielded saturating, CVD-free growth. The ALD Al_2O_3 timing sequence 50–70–50–70 was used for the remainder of the study. It is important to realize that these optimal ALD timing sequences are instrument-specific since they depend on the precursor partial pressures and residence times, the reactor geometry, and the amount of NanoDur substrate to be coated.

To further investigate the Al_2O_3 ALD on the calcined γ-Al_2O_3 nanoparticles, we used the timing sequence 50–70–50–70 and varied the number of ALD cycles between 0 and 90 [Fig. 3(b), inset]. A constant, linear weight gain was recorded from 6.6% after 5 cycles to ~119% after 90 cycles, indicating that the Al_2O_3 ALD proceeds without an incubation period on the NanoDur.[22]

B. Nanopore formation in ultrathin ALD films

After establishing the ALD timing sequences, 85 ALD TiO_2 cycles and 45 ALD Al_2O_3 cycles were performed on calcined γ-Al_2O_3 nanoparticles, yielding over-coating thicknesses of ~2.5 and ~4.9 nm, respectively. Our initial experiments focused on the TiO_2 over-coating since the XRD peaks arising from crystalline TiO_2 can be easily distinguished from the background peaks of the calcined Al_2O_3 substrate. The ALD TiO_2 sample was annealed to 1000 °C at a rate of 20 °C/min, and *in situ* SAXS measurements were recorded at ~100 °C intervals.[7] Figure 4(a) shows several representative SAXS intensity curves as a function of reciprocal space vector q (Å^{-1}) at different values of the annealing temperature. A change in the SAXS intensity may signify the formation of nanopores in the thin films and/or modification in the substrate.[7] We observed essentially no change in the SAXS intensity at annealing temperatures below ~400–500 °C [Fig. 4(a)]. However, an increase in SAXS intensity was observed in the region between 0.035 and 1 Å^{-1} at temperatures between 400–500 °C and 1000 °C [Fig. 5(b)]. We previously confirmed that the calcined γ-Al_2O_3 substrate was stable under the annealing conditions up to 1000 °C,[7] and so, it is safe to conclude that the changes in SAXS intensity signify changes in the TiO_2 over-coating.

Next, we subtracted the SAXS intensity data of the starting material recorded before anneal at room temperature from the SAXS data at elevated temperature. The background-subtracted data were fit using a spherical model to deduce the nanopore size distribution.[7] An average pore radius of 1.7 nm was computed from the pore size distribution at 530 °C. Upon further increasing the annealing temperature to 1000 °C, the pore radius increased continuously to 1.86 nm [Fig. 4(c)]. The pore radius decreased to ~1.65 nm during the 10 min hold at 1000 °C, suggesting that the 20 °C/min heating rate induced stress in the TiO_2 films that relaxed at 1000 °C. Strikingly, the pore radius remained essentially unchanged at ~1.65 nm during cooling at 20 °C/min to room temperature [Fig. 4(c)]. This result indicates that pore formation in ALD thin films is nonreversible. It should be noted that the formation and size of the pores might depend on parameters such as the heating rate, ALD film thickness, composition, crystallinity, and substrate.

We repeated the *in situ* annealing and SAXS experiments using the powder over-coated with ~4.9 nm ALD Al_2O_3, and the resulting average pore radius versus annealing temperatures is shown in Fig. 4(d) (see supplementary material, Fig. S1 for *in situ* SAXS measurements). Similar to the TiO_2 ALD films, pores were first observed in the ALD Al_2O_3 film at 400–500 °C with an average radius of 1.54 nm. As the temperature was increased from 500 to 1000 °C, the pore radius increased steadily to 1.86 nm [Fig. 4(d)]. The pore size remained constant at 1.86 nm as the temperature was lowered

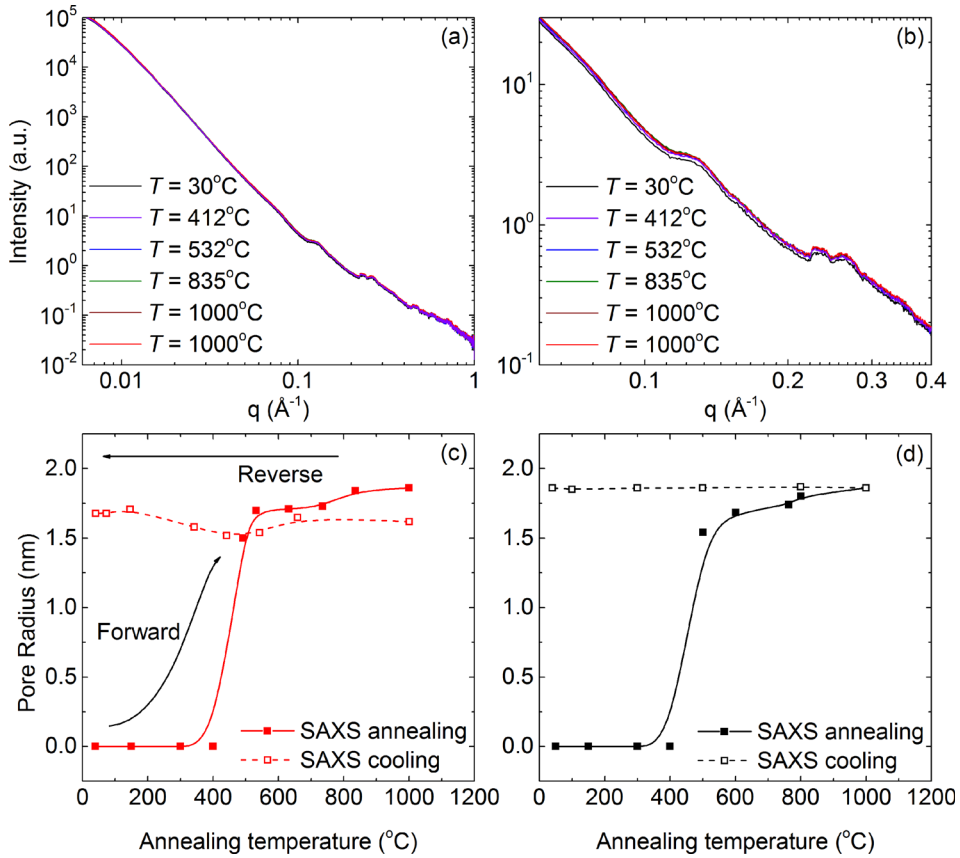

FIG. 4. (Color online) (a) Full range SAXS intensity data for 85 cycles of ALD TiO_2 over-coating on calcined γ-Al_2O_3 nanoparticles at different values of the annealing temperature. Nanopores emerge at ~400–500 °C. (b) Magnified graph of the 0.06–0.1 Å^{-1} region of the SAXS data vs reciprocal space vector q (Å^{-1}) showing an increase in SAXS intensity. Pore radius obtained from the SAXS data as a function of temperature for both forward (heating) and reverse (cooling) directions for (c) 85 cycles ALD TiO_2 over-coating and (d) 45 cycles ALD Al_2O_3 over-coating.

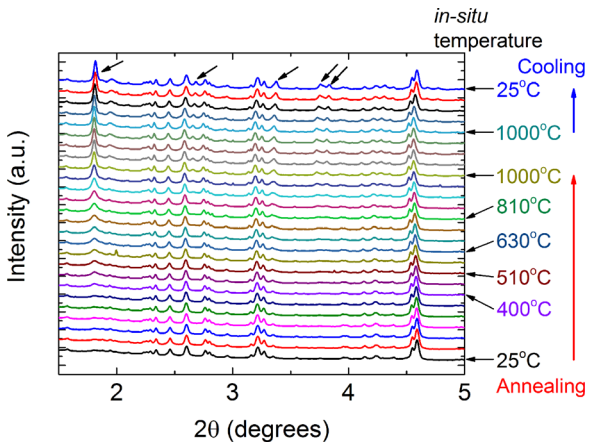

FIG. 5. (Color online) *In situ* XRD data for calcined γ-Al_2O_3 nanoparticles over-coated with 85 cycles of ALD TiO_2 vs temperature (black arrows reflect the measured diffractogram at the corresponding temperature). The appearance of new peaks (marked by black arrows) corresponding to the anatase TiO_2 phase can be seen at temperatures above 500 °C.

to room temperature [Fig. 4(d)]. These pore sizes are very close to the values measured previously by nitrogen adsorption measurements.[2] The absence of a decrease in the pore size during the 10 min hold at 1000 °C (as seen for TiO_2) suggests that no residual stress is imparted to the ALD Al_2O_3 film during annealing. The SAXS data for TiO_2 show more scatter as compared to Al_2O_3. This may result from the higher noise-to-signal ratio in the case of TiO_2 ALD films due to the lower thickness value of ~2.5 nm as compared to Al_2O_3 ALD films with a higher thickness value of ~4.9 nm.

As mentioned in the Introduction, pore formation in ALD thin films upon annealing is assumed to arise from densification produced by an amorphous to crystalline phase transition. To validate this hypothesis, *in situ* synchrotron XRD was employed to study phase changes in the ALD TiO_2 films upon annealing, and the diffraction patterns obtained at various temperatures are presented in Fig. 5. The black spectrum at the bottom in Fig. 5 shows the XRD pattern for calcined γ-Al_2O_3 nanoparticles over-coated with 85 cycles of ALD TiO_2. All the diffraction peaks correspond to γ-Al_2O_3, signifying that the NanoDur substrate particles did not convert to α-Al_2O_3 during calcination at 1000 °C in air for 3 h. This is somewhat surprising given that the γ-Al_2O_3 to α-Al_2O_3 phase transition in bulk Al_2O_3 occurs between 900 and 1000 °C.[19] The XRD peaks arising from the anatase and/or rutile TiO_2 phase were not observed in the 25 °C data signifying that the as-deposited ~2.5 nm TiO_2 ALD films are amorphous. Similarly, Ritala *et al.* found that ALD TiO_2 deposited using TTIP and H_2O grows in the amorphous phase at deposition temperatures below 225 °C on glass substrates.[12] As the annealing temperature increased to ~400–500 °C, new peaks appeared at $2\theta = 1.8°$, 2.68°, 3.37°, 3.76°, and 3.83° (black arrows in Fig. 5). These peaks correspond to the (101), (004), (200), (105), and (211) plane reflections of anatase TiO_2, respectively. This agrees well with the literature where ALD TiO_2 deposited at 450–500 °C was anatase (mass density of 3.84 g/cm^3).[18] As the annealing temperature increased to 1000 °C, the peak intensities also increased, signifying greater crystallinity. Strikingly, no rutile TiO_2 phase peaks were observed even at elevated temperatures of 1000 °C given that in bulk, the phase transition from anatase to rutile TiO_2 occurs at ~500–600 °C.[23] It should be noted that the reason to investigate the γ-Al_2O_3 nanoparticles over-coated with ALD TiO_2 is to study the phase transition in TiO_2 thin films (the new peaks in XRD can be easily distinguished from the substrate) and correlate it with the formation of pores in these films. For the Al_2O_3 ALD films, we observed that the amorphous films attained the same crystalline phase as the γ-Al_2O_3 substrate upon annealing and the phase transition cannot be distinctively marked.[7] However, it is plausible to assume that the phase transition in ALD Al_2O_3 films from amorphous [mass density of 3.0 g/cm^3 (Ref. 17)] to γ-Al_2O_3 (mass density of 3.65 g/cm^3, the same as the substrate (Ref. 19)] occurred at around 500 °C,[19] in-line with the SAXS measurements described earlier.

Subsequently, thermogravimetric analysis was performed on ~20 mg γ-Al_2O_3 nanoparticles bearing ALD TiO_2 or ALD Al_2O_3 over-coatings in order to quantify the mass loss. We observed a mass loss of roughly ~1.5% upon annealing at ~100–200 °C in both cases (Fig. S4), above which the mass loss was minimal. The mass loss upon annealing may relate to desorption of physisorbed moisture and/or removal of organic species. In view of these results, it is plausible to conclude that the amorphous to crystalline phase transition is the dominant factor that leads to the formation of nanopores, which occurs at much higher temperatures of 400–500 °C as aforementioned.

Having established that the formation of pores in ALD thin films is predominantly a consequence of an amorphous to crystalline phase transition and the associated densification, a mathematical model was constructed to further corroborate this finding (see Sec. II). The model is essentially based on induction of lateral stress in the ALD thin films arising from (1) step density increase at the phase transition temperature, and (2) thermal mismatch between the substrate and the film. All pores are assumed to be cylindrical and identical in shape and size. Since only one phase transition is observed in the investigated temperature range for both TiO_2 and Al_2O_3, it is plausible to assume that the density of the crystallized ALD films above the phase transition temperature ($T \approx 500$ °C) remains constant up to 1000 °C and the thermal mismatch is the dominant effect in this temperature range. Additionally, the phase transition and density changes are irreversible, and only stress due to the thermal mismatch relaxes upon cooling, in-line with the SAXS and XRD measurements. Figure 6(a) compares the pore radius values obtained from the model with the values obtained from SAXS for the 85 ALD TiO_2 cycle over-coating. The model shows good agreement with the SAXS data with only small deviations. It should be noted that the assumed mass densities may be inaccurate and that other mechanisms such as dehydroxylation and/or heating rate can affect the SAXS, which might explain the deviations. Upon cooling, the pore radius derived from the model is essentially constant signifying an irreversible process. Furthermore, Fig. 6(b) shows excellent agreement between the pore radius values derived from the model and the SAXS data for both

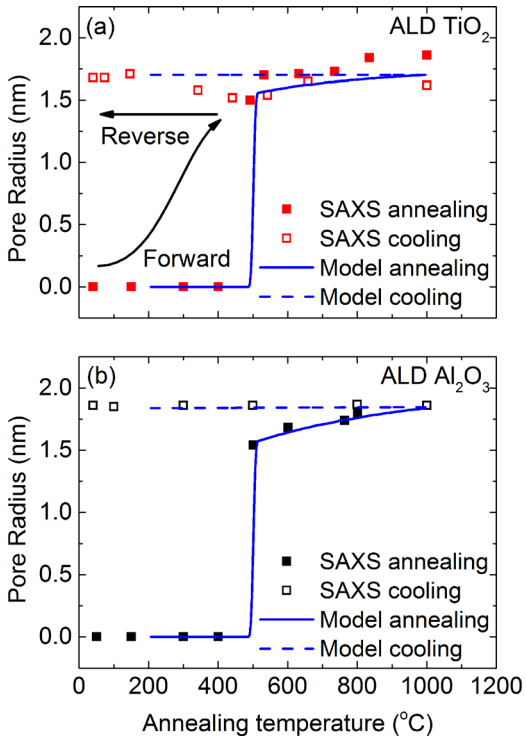

FIG. 6. (Color online) *In situ* SAXS data and mathematical model comparison for (a) 85 cycles of ALD TiO_2 over-coating and (b) 45 cycles of ALD Al_2O_3 over-coating on calcined γ-Al_2O_3 nanoparticles as a function of both forward and reverse temperatures.

forward and reverse scans, indicating that the assumed densities are in-line with our results. We also found that stress buildup in the ALD films due to densification from the phase transition is 5 orders of magnitude higher than that caused by the thermal mismatch so that densification dominates pore formation in these ultrathin ALD films.

IV. CONCLUSIONS

ALD TiO_2 and Al_2O_3 layers were grown on nonporous γ-Al_2O_3 nanoparticles to investigate the mechanism of pore formation during high temperature annealing. By means of *in situ* SAXS, we found that the pores formed abruptly at ~400–500 °C in both the TiO_2 and Al_2O_3 layers and that the pore size increases steadily with annealing temperature above 500 °C. *In situ* XRD measurements of ALD TiO_2 during annealing revealed that the amorphous to anatase TiO_2 phase transition occurs simultaneously with the formation of nanopores at ~400–500 °C. We propose that pore formation is primarily driven by relaxation of developed stress due to: (1) densification of ALD films because of phase transition and/or (2) thermal mismatch between the film and the substrate. A mathematical model constructed to evaluate this hypothesis yielded remarkable agreement with the nanopore sizes derived from SAXS. The understanding of size control of the nanopores gained in this work could be used to synthesize novel, supported metal nanoparticle catalysts with specific shape-selectivity. For instance, by selecting ALD over-coating films exhibiting a particular density change upon crystallization, we can tune the nanopore size to specific values that are optimal for a given shape selective catalytic process. In future studies, we hope to explore the effects of the ALD over-coat film thickness and the substrate composition on pore formation to gain further control over the pore size.

ACKNOWLEDGMENTS

This material is based upon work supported as part of the Institute for Atom-efficient Chemical Transformations (IACT), an Energy Frontier Research Center funded by the U.S. Department of Energy, Office of Basic Energy Sciences. The authors acknowledge the use of the Advanced Photon Source, an Office of Science User Facility operated for the U.S. Department of Energy (DOE), Office of Science by Argonne National Laboratory. This work was supported by the U.S. DOE under Contract No. DE-AC02-06CH11357. The authors would also like to thank Vincent Vandalon and Akhil Sharma (Eindhoven University of Technology) for fruitful discussion.

[1]J. Lu, J. W. Elam, and P. C. Stair, Acc. Chem. Res. **46**, 1806 (2013).
[2]J. Lu, B. Fu, M. C. Kung, G. Xiao, J. W. Elam, H. H. Kung, and P. C. Stair, Science **335**, 1205 (2012).
[3]H. Feng, J. Lu, P. C. Stair, and J. W. Elam, Catal. Lett. **141**, 512 (2011).
[4]B. J. O'Neill *et al.*, Angew. Chem. Int. Ed. **52**, 13808 (2013).
[5]A. C. Alba-Rubio *et al.*, ACS Catal. **4**, 1554 (2014).
[6]T. Li, A. J. Senesi, and B. Lee, Chem. Rev. **116**, 11128 (2016).
[7]T. Li, S. Karwal, B. Aoun, H. Zhao, Y. Ren, C. P. Canlas, J. W. Elam, and R. E. Winans, Chem. Mater. **28**, 7082 (2016).
[8]S. H. Jen, J. A. Bertrand, and S. M. George, J. Appl. Phys. **109**, 084305 (2011).
[9]S. H. Jen, S. M. George, R. S. McLean, and P. F. Carcia, ACS Appl. Mater. Interfaces **5**, 1165 (2013).
[10]J. W. Elam, M. D. Groner, and S. M. George, Rev. Sci. Instrum. **73**, 2981 (2002).
[11]J. A. Libera, J. W. Elam, and M. J. Pellin, Thin Solid Films **516**, 6158 (2008).
[12]M. Ritala, M. Leskela, L. Niinisto, and P. Haussalo, Chem. Mater. **5**, 1174 (1993).
[13]S. M. George, Chem. Rev. **110**, 111 (2010).
[14]J. Ilavsky and P. R. Jemian, J. Appl. Crystallogr. **42**, 347 (2009).
[15]L. D. Landau and E. M. Lifshitz, *Theory of Elasticity*, 2nd ed. (Pergamon, Oxford, 1986).
[16]P. Auerkari, *Mechanical and Physical Properties of Engineering Alumina Ceramics* (Technical Research Centre of Finland, Espoo, 1996).
[17]M. D. Groner, F. H. Fabreguette, J. W. Elam, and S. M. George, Chem. Mater. **16**, 639 (2004).
[18]M. Ritala, M. Leskelä, E. Nykänen, P. Soininen, and L. Niinistö, Thin Solid Films **225**, 288 (1993).
[19]I. Levin and D. Brandon, J. Am. Ceram. Soc. **81**, 1995 (1998).
[20]L. Borgese, M. Gelfi, E. Bontempi, P. Goudeau, G. Geandier, D. Thiaudière, and L. E. Depero, Surf. Coat. Technol. **206**, 2459 (2012).
[21]E. P. Meagher and G. A. Lager, Can. Miner. **17**, 77 (1979).
[22]J. W. Elam, J. A. Libera, T. H. Huynh, H. Feng, and M. J. Pellin, J. Phys. Chem. C **114**, 17286 (2010).
[23]O. Khatim, M. Amamra, K. Chhor, A. M. T. Bell, D. Novikov, D. Vrel, and A. Kanaev, Chem. Phys. Lett. **558**, 53 (2013).
[24]See supplementary material at http://dx.doi.org/10.1116/1.5003360 for expected weight gain calculations, in-situ SAXS of Al_2O_3 ALD over coating, mathematical model and thermogravimetric analysis.